LA-UR-86-3765 J. PHYS. C 20 2361 (1987)

KINK-ANTIKINK SCATTERING FOR AN EASY-PLANE ONE-DIMENSIONAL ANTIFERROMAGNET

G. M. Wysin and A.R. Bishop

Los Alamos National Laboratory
Los Alamos, New Mexico 87545

Abstract

A numerical investigation of collisions of kink-antikink ($K\bar{K}$) pairs in an easy-plane classical antiferromagnetic chain is presented here, for the case of an applied field within the easy plane. An approximate kink profile as obtained from an earlier Ansatz was used as the initial condition for numerical integration on a discrete lattice. As a function of the applied magnetic field and kink Ansatz parameter θ_A, which measures the tilt of the spins out of the easy plane, we have found distinct parameter regimes resulting in transmission, reflection, and annihilation of the $K\bar{K}$ pair. Results for both the in-plane (XY) and out-of-plane (YZ) kinks are summarized, and comparison is made to $K\bar{K}$ scattering in the easy-plane ferromagnet. Similarly to the case of the easy-plane ferromagnet $CsNiF_3$, it is found that these results imply difficulties in the interpretation of experiments on tetramethyl ammonium manganese trichloride (TMMC) in terms of classical soliton theory. For example, for fields from approximately 20 kG to 80 kG, the low velocity XY collisions generally result in pair annihilation to spin waves. For fields less than 20 kG, however, the low velocity $K\bar{K}$ XY pair transmits. Experimental results for TMMC are discussed in the light of these features.

1. *Introduction: Solitons in One-Dimensional Magnets*

There are a number of unresolved questions concerning the theoretical description of magnetic chain materials. In particular we consider those expected to support sine-Gordon soliton-like excitations (which we refer to here as kinks). Typical examples of these materials include easy-plane ferromagnets (EPF's) $CsNiF_3$ (spin S=1), $(C_6H_{11}NH_3)CuBr_3$, or "CHAB" (S=1/2), and the easy-plane antiferromagnet (EPA) $(CD_3)_4NMnCl_3$, or TMMC (S=5/2). In the presence of an applied magnetic field within the easy plane, a classical mechanics description using a nearest neighbour Hamiltonian with either exchange or single ion anisotropy leads approximately to a sine-Gordon (SG) equation of motion for the in-plane spin angle ϕ (Mikeska 1978,1980). This approximate equation of motion requires the assumptions of slow spatial variations in the spin fields or sublattice spin fields for the antiferromagnet (continuum limit), small out-of-easy-plane spin motions, and of course supposes classical mechanics to be adequate. Generally, for small enough applied field and velocity, the predicted kink width will be small enough so that the continuum limit is a good approximation. While the out-of-plane angle θ may be fairly small for some slowly moving kinks, it nevertheless introduces terms in the equations of motion ignored in the SG treatment (beyond terms linear in θ), which typically cannot be neglected for an accurate evaluation of the energy-velocity dispersion E(v).

In fact, these terms can have a dramatic effect, changing the solutions qualitatively from the SG limit. For sufficiently large applied fields, greater than an anisotropy-dependent critical field B_c (Kumar 1982, see also Harada *et al* 1981), the easy-plane SG-like kinks acquire a negative effective mass, regardless of whether the

continuum limit was used (Wysin *et al* 1984,1986). For ferromagnetic (FM) coupling, these high field kinks have been shown numerically to *reflect* as a result of $K\overline{K}$ collisions-- i.e., collisions of kink-antikink pairs of equal but opposite velocity (Wysin *et al* 1984). At fields below the critical field, the FM $K\overline{K}$ pair can either transmit (at the smallest fields), annihilate (at intermediate fields), or reflect (at fields just below the critical field). This behaviour would not be expected in a pure SG system--only transmission of the pair could occur if the SG dynamics were a good approximation to the dynamics of the original complete Hamiltonian. These discrepancies can be traced to the terms in the magnetic Hamiltonian which are inherently nonlinear degrees of freedom (the out-of-plane angles), but which are approximated as linear degrees of freedom to obtain the SG Hamiltonian. The SG equation of motion includes the nonlinear dynamics of the in-plane angle ϕ, while the out-of-plane angle θ essentially becomes its conjugate momentum (i.e. $\theta \approx \dot{\phi}$), an approximation which generally turns out to be inaccurate. These additional terms in the Hamiltonian also introduce non-zero frequency bound states in the kink spectrum which are responsible for the non-SG behaviour of the collisions.

A study of $K\overline{K}$ collisions in the easy-plane *antiferromagnet* (AFM) is a natural extension of the above mentioned work. This study is similar to that for the ferromagnet, with the major difference being the need to include kinks from both the *XY* and *YZ* regimes of the dispersion curve (Flüggen and Mikeska 1983). We accomplished this in a natural way by employing a previously introduced Ansatz for the kink profile as the initial condition for the numerical integration (Wysin 1985, Wysin *et al* 1986). The kink changes smoothly from *XY* in character (small z spin components) to

YZ (small x spin components) as a variational parameter θ_A (which measures the out-of-plane tipping) is increased from zero towards $\pi/2$.

A priori it was not at all clear whether AFM $K\overline{K}$ scattering should resemble $K\overline{K}$ scattering in the FM. Here we have found some similarities between the two, especially if one considers the XY AFM kinks to be analogous to the FM kinks. The analogy can also be seen in the dispersion relationships for isolated kinks. Here we will review the single kink dispersions and present new $K\overline{K}$ data to support this view.

We do not address the question of the adequacy of a classical mechanics vs. quantum mechanics description. Certainly if these spin systems are strongly quantum mechanical, then it is necessary to re-examine what is meant by "quantum soliton", especially since the SG soliton limit for these one-dimensional (1D) magnets is derived from a classical analysis. Quantum aspects of this problem have been partially studied in other articles. For example, Mikeska and Frahm (1986) and Fogedby *et al* (1986) have applied the semiclassical approximation for large spin to the quantum specific heat problem. The quantum corrections to the classical SG model have been reviewed by Johnson and Wright (1985); they point out that for the specific heat of CHAB and TMMC these corrections increase the disagreement of the theory with experiment, and cause only a slight improvement in the decription of the specific heat of $CsNiF_3$. On the other hand, classical calculations using the full magnetic Hamiltonian for $CsNiF_3$ (e.g. transfer matrix calculation of Pini and Rettori 1984) or for TMMC (e.g. Monte Carlo calculation of Jensen *et al* 1985) have demonstrated difficulties also in a classical description of these materials. Generally these classical calculations overestimate the magnitude of specific heat peaks when compared to experiment. It seems likely

that quantum effects restrict the spin motions more strongly than expected to the easy plane, thereby reducing the effective number of degrees of freedom, and making classical SG theory more appropriate than the full magnetic Hamiltonian theory. Emerging "numerically exact" quantum transfer matrix calculations for S=1/2 (Wysin and Bishop 1986) also show this reduction in the effective number of degrees of freedom-- quantum transfer matrix specific heat peaks have close to the same magnitude as experiment and classical SG theory for CHAB. Since this question is not completely resolved even for static (thermodynamic) properties, especially for S=5/2 TMMC, investigation of classical AFM $K\bar{K}$ dynamics clearly is a useful tool.

The stability properties of the *XY* and *YZ* kinks are relevant for determining the allowed initial conditions. These stability regimes have already been established, partly numerically and partly by a linear stability analysis (Wysin *et al* 1986, see also Lemmens *et al* 1986 for an alternative view). These will be reviewed below in Section 2, along with the dispersion relations. In Section 3A we shall give a brief description of the numerical method and analysis, and a review of the FM $K\bar{K}$ results. In Section 3B we present the new AFM $K\bar{K}$ results, in terms of the three regimes labeled on dispersion curves and on a final state output "phase diagram". The similarities to FM $K\bar{K}$ collisions will be noted, and the relevance of these results to TMMC experiments will be discussed in Section 4.

2. *Review of Single Kink Dynamics*

The nearest-neighbour Hamiltonian under consideration here includes an applied easy-plane field $B = B_x$, and single ion anisotropy $A > 0$;

$$H = \sum_{n=1}^{N} [J \mathbf{S}_n \cdot \mathbf{S}_{n+1} + A (S_n^z)^2 - g \mu_B B^x S_n^x], \tag{1}$$

where $J > 0$ is the nearest-neighbour exchange ($J \approx 6.5$ K and $A/J \approx 0.04$ for TMMC, Regnault *et al* 1982), n labels the lattice sites, and μ_B is the Bohr magneton, and the xy plane is the easy plane. The continuum limit SG equations of motion derived from this Hamiltonian were given originally by Mikeska (1980), and Flüggen and Mikeska (1983). Later they were re-analyzed by Wysin *et al* (1986), who found that using a coordinate system with the x axis as the polar axis allows a more natural description of YZ kinks, while at the same time simplifying their stability analysis. Note that for the numerical integration presented here, it is most convenient to apply the discrete equations of motion in terms of xyz spin components rather than angles, *i.e.*,

$$\dot{\mathbf{S}}_n = \mathbf{S}_n \times [-J (\mathbf{S}_{n-1} + \mathbf{S}_{n+1}) + g \mu_B \mathbf{B} - 2A S_n^z \hat{\mathbf{z}}], \tag{2}$$

since this allows for integration of the 3N equations of motion without the evaluation of any trigonometric functions. In this way spin length and energy conservation both serve as checks of the numerical accuracy. (Note that there is no damping in this simulation.)

The energy-velocity dispersion relation for isolated kinks has been determined by three different methods:

i) approximately from the SG limits, both XY and YZ;

ii) by numerical integration of the discrete equations of motion, using an appropriate

initial condition (either SG-like or from the Ansatz, below), combined with a time averaging procedure to remove spin waves;

iii) by applying a variational Ansatz, that assumes simple profiles for the spins on both the even and odd sub-lattices, as being SG profiles in tilted spin-space coordinates (Wysin *et al* 1986).

These all give similar qualitative results for the *XY* and *YZ* branches, however, the latter two show that the *XY* branch terminates where it meets the *YZ* branch, an important detail which is lost in the SG approach. Furthermore, the SG limit drastically overestimates the effective mass for *XY* kinks.

The numerical method directly gives stability information (Wysin *et al* 1986). Combined with a linear stability analysis for *YZ* kinks, it has been demonstrated that *YZ* kinks have a limited range of stability. At fields less than the critical field B_c, only *YZ* kinks with velocities greater than some minimum value v* will be dynamically stable. If the field is equal to B_c, the minimum velocity v* approaches zero. For fields greater than the critical field, v* becomes negative. This is shown more clearly in Fig. 1; also see Wysin *et al* (1986) for a further explanation of *YZ* kink stability. At the same time, as the applied field is varied from below to above B_c, the *XY* branch continuously diminishes to a point (for $B = B_c$), and re-emerges with downward curvature (implying negative effective mass) for fields greater than B_c. These negative effective mass *XY* kinks are also dynamically stable, as demonstrated in these numerical integrations.

The limited extent of the *XY* branch could be interpreted to mean that SG-like *XY* kinks with larger (absolute value) velocities are dynamically unstable. Note that it is possible to estimate the stability limit for the *XY* kinks from the linear stability analysis for *YZ* kinks, since the two dispersion curves end where they intersect. A linear stability analysis can be performed for moving as well as stationary SG-like *YZ* kinks: First order perturbation theory for the moving *YZ* kink linear stability problem estimates the velocity v* at which the *XY* branch meets the *YZ* branch, as (Wysin *et al* 1986)

$$v^*/c_0=\frac{2}{\pi}\frac{B_c}{B}[1-(\frac{B}{B_c})^2], \tag{3a}$$

where

$$c_0=2JS/\hbar\ , \tag{3b}$$

and the critical field is

$$B_c=[8AJS^2]^{1/2}/(g\mu_B). \tag{4}$$

The lattice spacing is used as the unit of length here. Note that for $B<B_c$, when $v^*>0$, the *XY* effective mass is positive, while for $B>B_c$, when $v^*<0$, the *XY* effective mass is negative. Equation (3a) is an approximate expression which is most accurate for B near B_c. Also note that one cannot determine v* by equating the predicted SG *XY* and *YZ* energies for a given field; the SG theory predicts that the branches do not cross except for B very near B_c. The non sine-Gordon behaviour manifests itself by strongly changing the effective masses of the *XY* kinks.

The *XY* kinks are in many ways analogous to the kinks of the easy-plane ferromagnet. The EPF kink's effective mass changes sign at a corresponding critical

field, the absolute values of the effective masses are much smaller than predicted by SG theory, and they are also *dynamically* stable even for fields greater than the critical field. And while the *XY* kinks obey dynamics very different from SG-like, the *YZ* kinks, on the other hand, can be described quite accurately using SG dynamics outside of the unstable regimes mentioned. The EPA *YZ* kinks have no natural analogue in the ferromagnet.

With the above points in mind, we can hope that these EPA $K\overline{K}$ numerical collision experiments will answer the following questions:

i) Generally, what outcomes are possible for EPA $K\overline{K}$ collisions, of either *XY* or *YZ* type?

ii) Is the behaviour of *XY* $K\overline{K}$ collisions similar to that of the $K\overline{K}$ collisions of the EPF?

iii) How do we characterize the behaviour of *YZ* $K\overline{K}$ collisions?

To prepare for the presentation of our results, we first review the EPF $K\overline{K}$ scenario.

3. Kink-Antikink Collisions

3A. Ferromagnetic $K\overline{K}$ Method and Results

The main features of EPF $K\overline{K}$ collisions have been given earlier (Wysin *et al* 1984). The numerical method used for either ferro- or antiferro-magnetic coupling is essentially the same. The method used for the ferromagnet will be reviewed next, and modifications necessary to study the antiferromagnet will be described later.

The discrete equations of motion for the EPF were integrated numerically on a lattice of 80 to 180 spins, a larger number being necessary for kinks of greater width

(where the kink width $w = \sqrt{JS/g\mu_B B}$). The initial condition was taken to be a single SG kink profile, corresponding to an SG velocity v_{SG}. By using Neumann boundary conditions for the *xyz* components, the kink interacts with its mirror image opposite velocity antikink at the boundary. In this way we need only half as many lattice points as compared to using a SG $K\bar{K}$ profile on a lattice with periodic boundary conditions, in addition to saving a factor of two in CPU time. The Numerical method was a standard fourth order Adams-Bashforth-Moulton predictor-corrector scheme with mop-up. (For example, see Ceschino and Kuntzmann 1966.) The profile was allowed to evolve until approximately twice the time for the kink to reach the boundary. By viewing the time evolution of the profile and spatial averages (denoted with < >) of the in-plane and out-of-plane angles, it was possible to classify the final state according to whether the $K\bar{K}$ pair underwent

i) SG-like transmission, with monotonically increasing or monotonically decreasing $\langle\phi\rangle(t)$; or

ii) reflection, with a reversal of the slope of $\langle\phi\rangle(t)$; or

iii) breather formation or annihilation, with oscillatory $\langle\phi\rangle(t)$.

The final state was found to be dependent on both the initial SG velocity v_{SG} and the applied field (for a fixed value of anisotropy ratio A/J). Results are summarized in Figure 4 of Wysin *et al* (1984), in terms of an output state phase diagram with four different regimes. The SG-like transmission regime covers only a small portion of the diagram--generally the collision behaviour is unlike sine-Gordon dynamics. Regimes III and IV in the figure both involve $K\bar{K}$ reflection. However, in regime IV negative effective mass kinks reflect with no change in velocity, while in regime III positive

effective mass kinks reflect, *with a velocity change* (but no change in energy; there are two types of regime III kinks with equal energy but different velocity). Also, a detail not illustrated in the breather formation regime of Figure 4 (Wysin *et al* 1984) is the existence of at least one SG-like transmission window. With such a rich variety of non-SG behaviour for these equal but opposite velocity collisions, we also expect a similar variety for unequal velocity $K\bar{K}$ pairs.

3B. EPA $K\bar{K}$ Collisions

For this case we used 101 to 501 lattice sites, with the kink width varying as $w \approx 2JS/(g\mu_B B)$ for XY kinks and as $w \approx \sqrt{J/(2A)}$ for YZ kinks. Using a fixed ratio $2A/J=0.04$, the field ranged from $B/B_c=0.10$ to $B/B_c=1.50$. For TMMC, this corresponds to $9.0\ kG \le B \le 140\ kG$, with $B_c \approx 90\ kG$. The initial condition was an Ansatz profile for some specified value of a parameter θ_A, where θ_A determines the tilt of the spins out of the easy plane on the A-sublattice (Wysin *et al* 1986). The resulting profile could correspond to either an XY or YZ kink, depending on whether θ_A was near zero or $\pi/2$. At some intermediate value of θ_A, the Ansatz kink switched from the XY branch to the YZ branch. A given combination of θ_A and B/B_c then determined the initial velocity, energy, and width of the kink.

Neumann boundary conditions were applied to the xyz spin components, but now the spatial derivatives on each sublattice were separately set to zero at the boundaries. Integration proceeded until about twice the time necessary for the kink to interact with its mirror image antikink at the boundary. Classification of the type of collision was based on viewing the time evolution of the spin profile and the spatial averages of in-plane and out-of-plane angles. The tilt of the two spins at the center of one kink, one

on each sublattice, measured from the easy plane, provided another diagnostic.

Possible outcomes of collisions include SG-like transmission, annihilation, and reflection. Typical cases of each of these are shown in Figures 2-6. The profiles are viewed in either z-polar or x-polar spherical coordinates, depending on which was visually more convenient. These results are summarized in Figures 7,8 and 9, as indicated on the single kink dispersion curves. An alternative representation of the summarized data is the final state phase diagram of Figure 10.

The results for low velocity XY kinks are similar to those for ferromagnetic kinks. Generally, for low fields $B < 0.2B_c$ there is SG-like transmission. At higher fields but still with $B < B_c$ the low velocity pairs annihilate, or possibly form breathers, and the higher velocity XY kinks undergo SG-like transmission. For $B > B_c$, the negative effective mass XY kinks reflect, as in the ferromagnet. Most of the cases tested for YZ $K\bar{K}$ pairs resulted in transmission, consistent with their nearer to SG behaviour. The exceptions included some cases at small velocity for $B > B_c$, where annihilation occurs. Other annihilation cases, at the XY to YZ boundaries for $B > B_c$ may be artifacts of the Ansatz initial condition.

4. Discussion

Typically the dynamic behaviour of isolated kinks in easy-plane magnets has been seen to be only poorly described by a sine-Gordon equation. Generally the effective kink mass is modified by additional terms in the equations of motion not included in the simplified SG picture. These additional terms also are responsible for introducing internal bound states in the kink spectrum which are very important for collisions. In

the extreme case of applied fields greater than the critical field, the effective mass can be negative, a result of an instability that changes the character of the kink but does not destabilize it. The collisions of equal but opposite velocity ferromagnetic $K\overline{K}$ pairs has been seen to be drastically different from simple SG transmission. Outcomes can additionally include annihilation and reflection. These statements also apply to the easy-plane antiferromagnet, especially for the XY kinks, which in some ways are analogous to the EPF kinks. For both the EPF and EPA $K\overline{K}$ collisions, low field nearly planar kinks (xy-like) undergo transmission, while for larger fields the behaviour generally changes from annihilation to reflection as the field increases.

The existence of large ranges of applied field for which annihilation occurs may raise a problematic issue for the interpretation of neutron scattering experiments on TMMC (Boucher *et al* 1983). If $K\overline{K}$ collisions in the sample in thermodynamic equilibrium tend towards annihilation, then the previously assumed noninteracting kinks no longer can be considered as stable fundamental excitations of the system. Rather, spin waves and multi spin waves would predominate and determine the spectra and thermodynamic properties. However, the classical SG theory agrees well with neutron scattering data for TMMC---no sign of a collisional kink instability is indicated. In light of the results presented here, and similarly for $CsNiF_3$, this is a confusing point-- clearly, we need to better understand the thermal distribution of XY and YZ kinks.

It is possible that such a good fit to SG theory is primarily a consequence of quantum effects. A quantum approach may show that the spins are strongly restricted to the easy plane, more so than in the classical theory, making SG theory a reasonable

approach. Indeed, there is already indirect support for this view (Tinus *et al* 1985,1986, also see Wysin and Bishop 1986) in the EPF CHAB and possibly also in $CsNiF_3$. Quantum restriction to the easy plane is indicated even in the *semiclassical* calculations for EPF's of Mikeska and Frahm (1986) and Fogedby *et al* (1986), although these do not completely bring theory into agreement with experiment. Exact quantum calculations, for both thermodynamics and statistical mechanics, will most likely be necessary to clarify the theory for TMMC just as for EPFs.

References

Boucher J P, Regnault L P, Rossat-Mignod J, Renard J P, Bouillot J, Stirling W G and Mezei F 1983 *Physica* **120B** 241

Ceschino F and Kuntzmann J 1966 *Numerical Solution of Initial Value Problems* PrenticeHall

Flüggen N and Mikeska H J 1983 *Solid State Commun.* **48** 293

Fogedby H C, Osano K and Jensen H J 1986 preprint

Harada I, Sasaki K and Shiba H 1981 *Solid State Commun.* **40** 29

Jensen H J, Mouritsen O G, Fogedby H C, Hedegård P and Svane A 1985 *Phys. Rev.* **B32** 3240

Kumar P 1982a *Phys. Rev.* **B25** 483

------ 1982b *Physica* **5D** 359

Lemmens L F, Kimura I and de Jonge W J M 1986 *J. Phys. C: Solid State Phys.* **19** 139

Mikeska H J 1978 *J. Phys. C: Solid State Phys.* **11** L29

------ 1980 *J. Phys. C: Solid State Phys.* **13** 2913

Mikeska H J and Frahm H 1986 preprint *J. Phys. C: Solid State Phys.*

Pini M G and Rettori A 1984 *Phys. Rev.* **b29** 5246

Regnault L P, Boucher J P, Rossat-Mignod J, Renard J P, Bouillot J and Stirling W G 1982 *J. Phys. C: Solid State Phys.* **15** 1261

Tinus A M C, de Jonge W J M and Kopinga K 1985 *Phys. Rev.* **B32** 3154

------ 1986 *J. Magn. Magn. Mat.* **54-57** 824

Wysin G M 1985 *PhD Thesis* CornellUniversity

Wysin G M and Bishop A R 1986 *Phys. Rev.* **B34** 3377

Wysin G, Bishop A R and Kumar P 1984 *J Phys. C: Solid State Phys.* **17** 5975

Wysin G M, Bishop A R and Oitmaa J 1986a *J. Phys. C: Solid State Phys.* **19** 221

------ 1986b *J. Magn. Magn. Mat.* **54-57** 831

Figure Captions

Fig. 1. Some typical EPA kink energy-velocity dispersion relationships, at three different fields. The data points were obtained from numerical integrations with A/J=0.02, and B/B_c = 0.75 (□), 1.0 (Δ), and 1.25 (×). The curves are the corresponding results from a variational Ansatz calculation. The energy is measured in units of JS^2, and the velocity in units of $JS/\hbar$.

Fig. 2. $K\bar{K}$ collision of an XY-like pair, resulting in SG-like transmission; at field B/B_c=0.25, with initial velocity v_0=1.4 (or θ_A=0.180243). The angle ϕ within the easy plane (on one sublattice) is shown in (a), and the associated out of easy plane angle θ is shown in (b). The time evolution of the spatial average of the in-plane angle, $\langle\phi\rangle(t)$, is shown in (c). Theta-A and theta-B in (d) are the out of easy plane tilting of the two spins, one on each sublattice, at the center of the kink vs. time. Note that in this case theta-A and theta-B interchange during the collision.

Fig. 3. $K\bar{K}$ collision of an XY-like pair resulting in annihilation; at field B/B_c=0.25, with initial velocity v_0=0.37 (or θ_A=0.024673). Parts (a) through (d) are as described in Fig. 2. Note the oscillations, suggestive of formation of a breather-like bound state.

Fig. 4. $K\bar{K}$ collision of an XY-like pair resulting in reflection; for B/B_c=0.75, with v_0=0.59 (θ_A=0.932563). Parts (a) through (d) are as described in Fig. 2. Note that theta-A and theta-B change sign during the collision, as does the slope of $\langle\phi\rangle(t)$.

Fig. 5. $K\bar{K}$ collision of an XY-like pair also resulting in reflection, but for B/B_c=1.075, with v_0=0.06 (θ_A=0.364563). Parts (a) through (d) are as described in

Fig. 2. Again theta-A and theta-B change sign during the collision, but one passes through zero and the other passes through π in the process.

Fig. 6. $K\bar{K}$ collision of a YZ-like pair, resulting in SG-like transmission, for B/B_c=0.75, with v_0=0.73, (θ_A=1.59537). In this figure, ϕ and θ in parts (a) and (b) are the angles within the yz-plane and out of the yz-plane respectively, for one sublattice. In (c), $\langle\phi\rangle$ is the spatial average of ϕ in the yz-plane. In (d), however, theta-A and theta-B are the out of easy plane tilting for the two spins at the center of the kink, one for each sublattice, as in Figures 2-5.

Fig. 7. $K\bar{K}$ output states in an energy (in units of JS^2) vs. velocity (in units of $JS/\hbar$) representation, for A/J=0.02, and applied fields B/B_c=0.10 (solid curve), 0.175 (dashed curve), 0.25 (dotted curve) and 0.375 (chain-dot curve). The data symbols refer to individual $K\bar{K}$ simulations resulting in SG-like transmission (Δ) or annihilation ($\times$).

Fig. 8. $K\bar{K}$ output states in the energy-velocity representation, for A/J=0.02, and applied fields B/B_c=0.5 (solid), 0.625 (dashed), 0.75 (dotted) and 0.925 (chain-dotted). The symbols refer to transmission (Δ), annihilation ($\times$) and reflection ($\bullet$).

Fig. 9. $K\bar{K}$ output states in the energy-velocity representation, as in Fig. 8, for (a) B/B_c=1.0, (b) B/B_c=1.075, (c) B/B_c=1.25, and (d) B/B_c=1.375. The backwards branch, negative effective mass XY kinks always reflect; the YZ kinks generally transmit.

Fig. 10. An output state "phase diagram" in terms of the applied field B/B_c and the Ansatz parameter θ_A (approximately equal to the tilt of the spins out of the easy

plane at the kink center). The symbols refer to transmission (Δ), annihilation (×) and reflection (●).

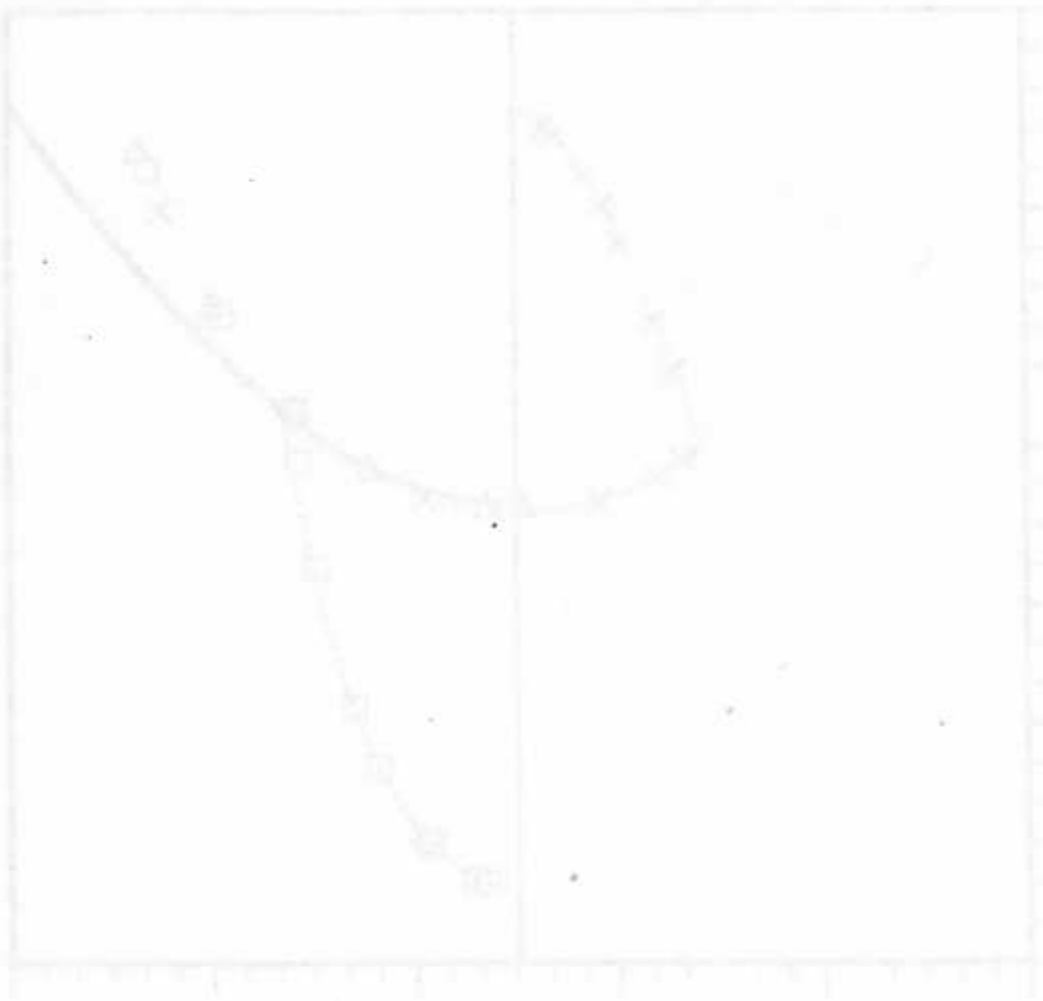

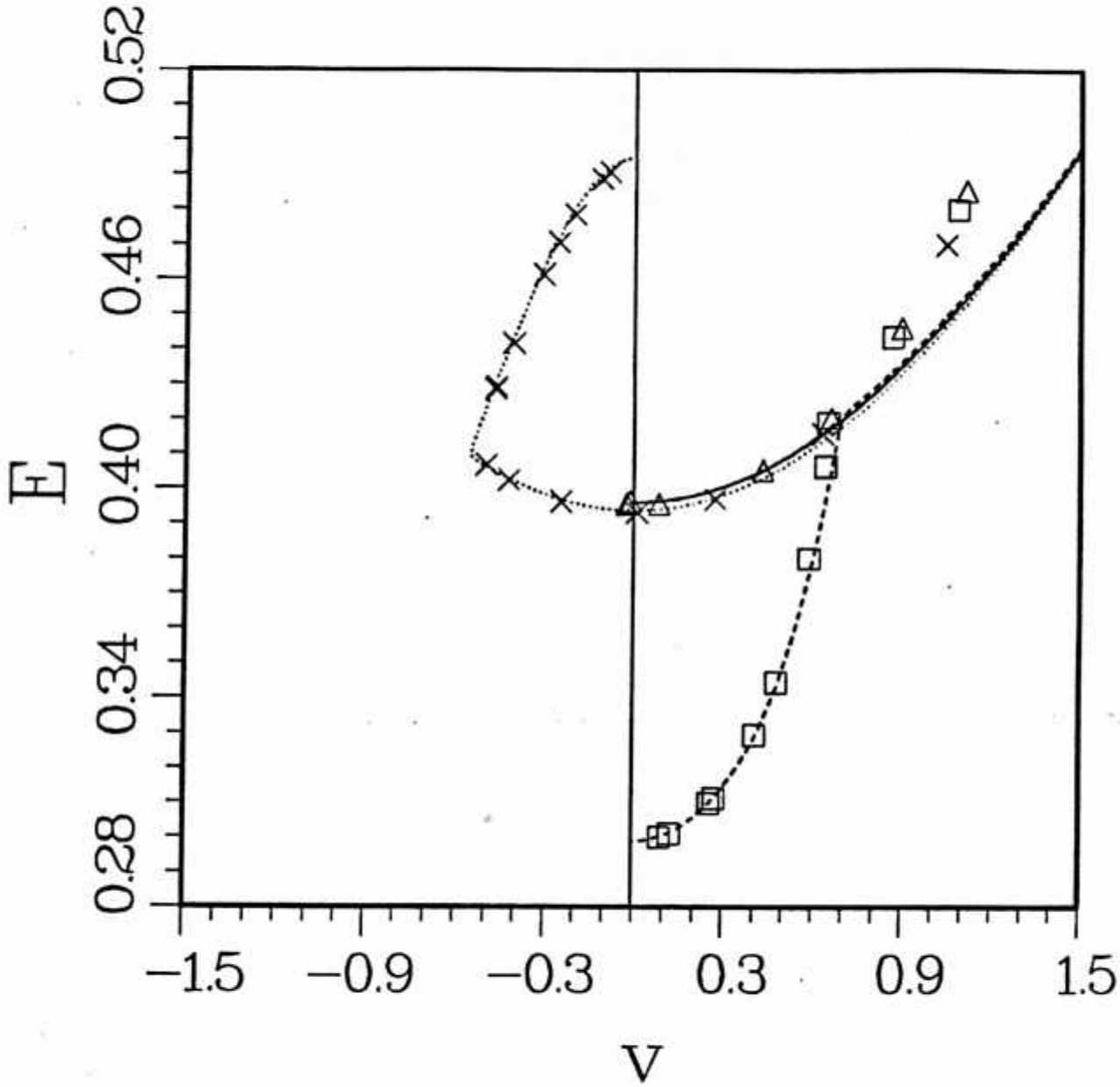

FIG. 1.

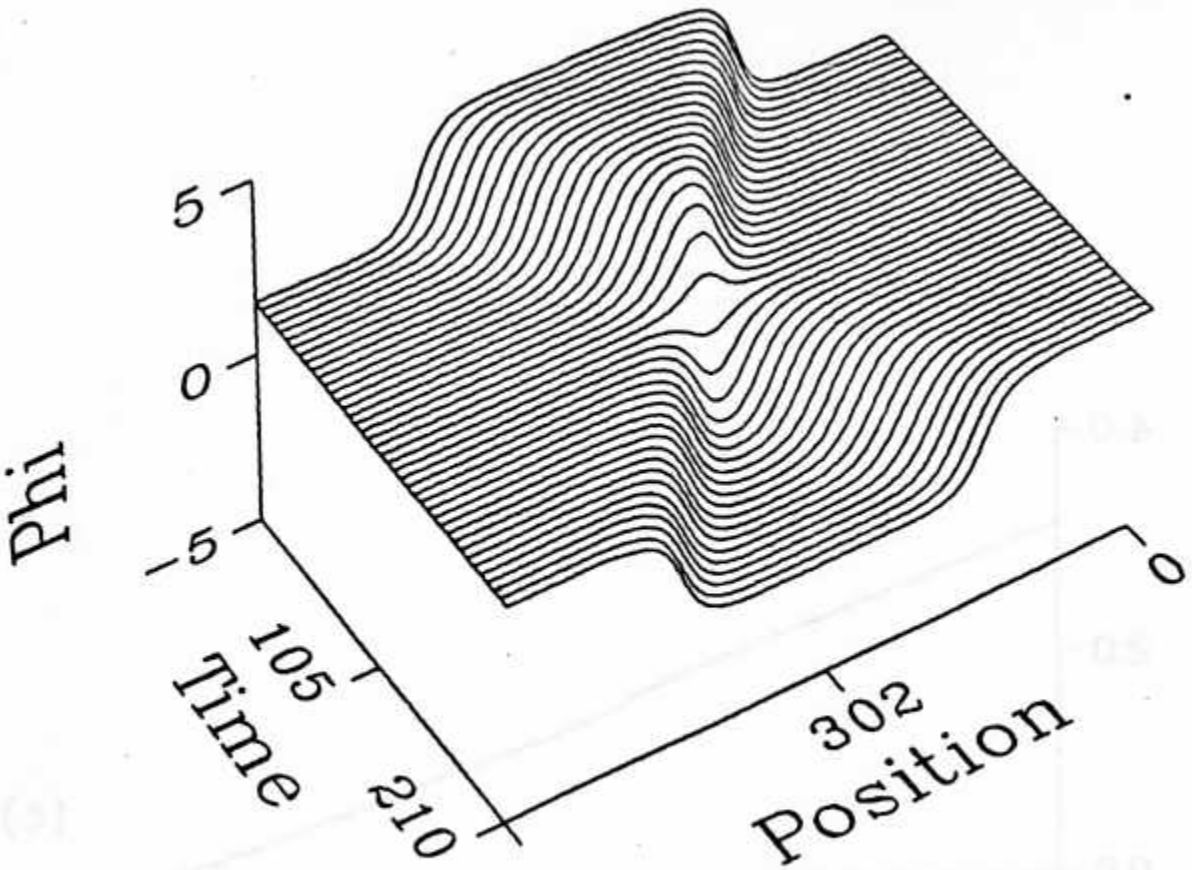
Phi
5
0
-5
Time
105
210
302
Position
0
(a)

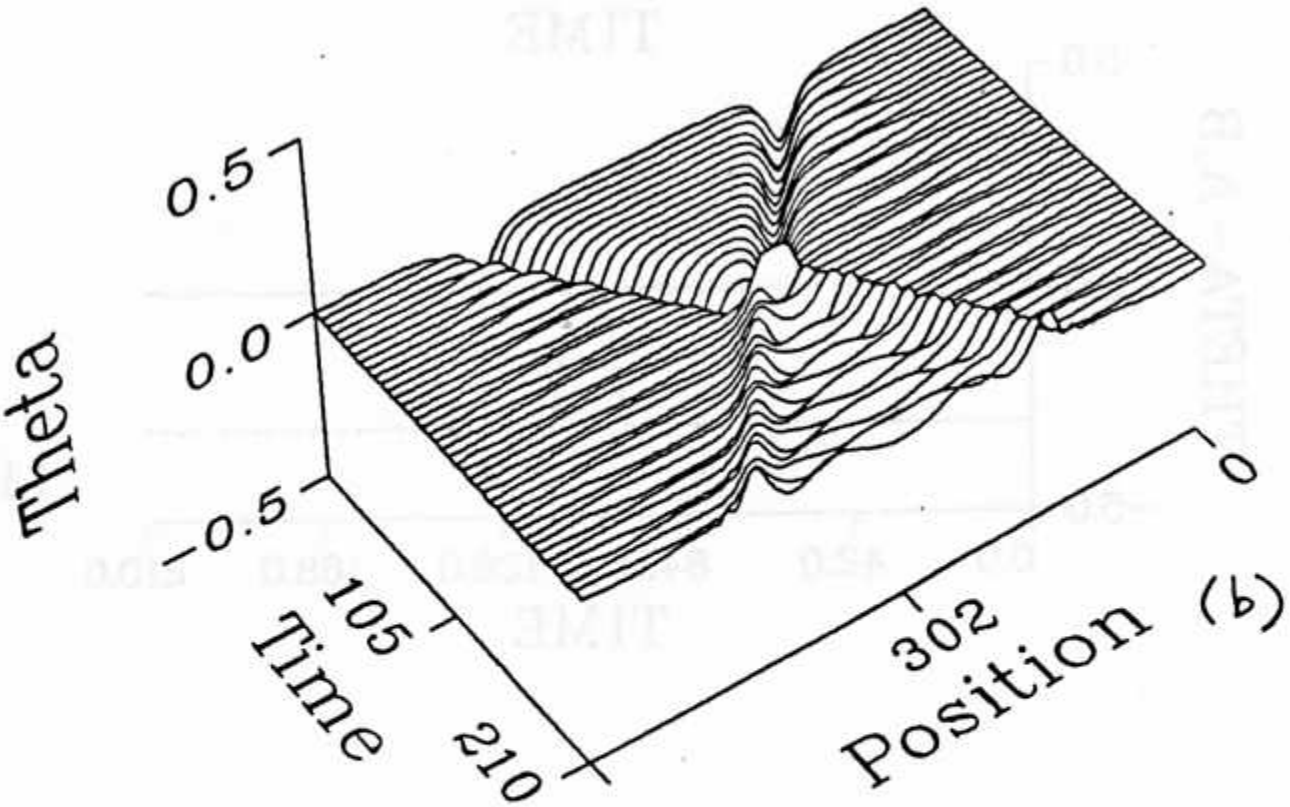
Theta
0.5
0.0
-0.5
Time
105
210
302
Position
0
(b)

FIG. 2.

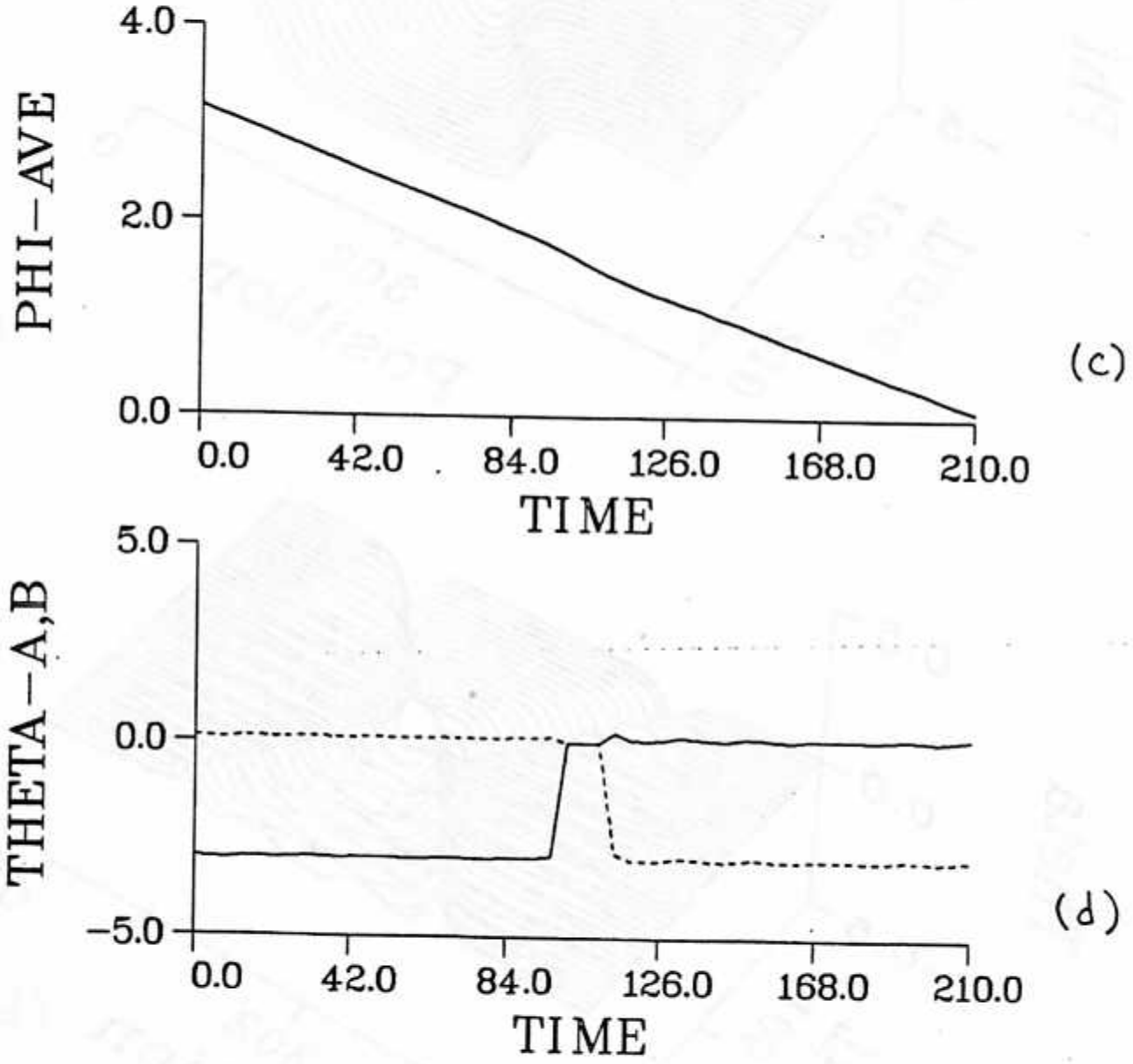
PHI–AVE
4.0
2.0
0.0
0.0
42.0
84.0
126.0
168.0
210.0
TIME
(c)
THETA–A,B
5.0
0.0
–5.0
0.0
42.0
84.0
126.0
168.0
210.0
TIME
(d)

FIG. 2.

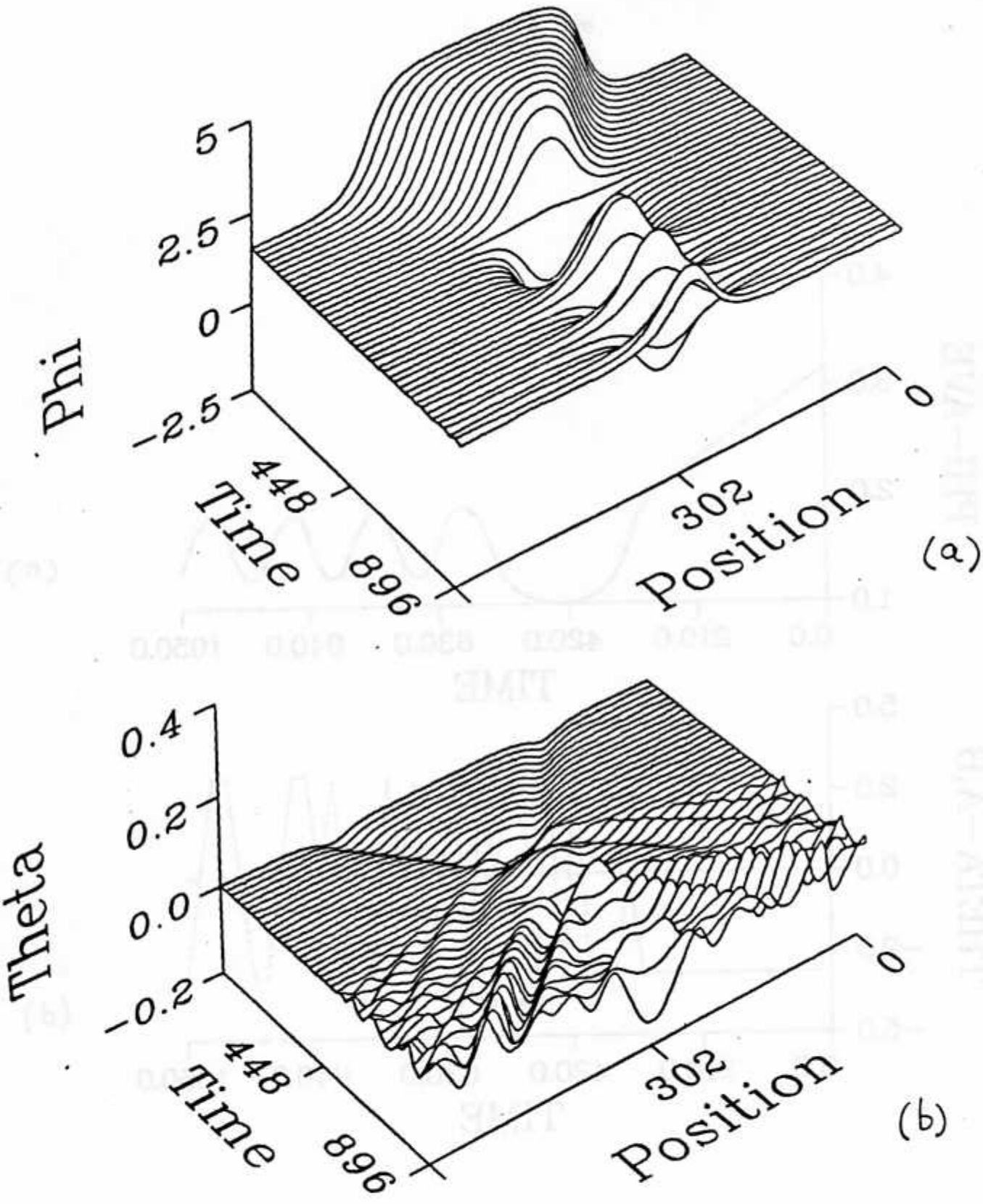
Phi
5
2.5
0
-2.5
448
Time
896
302
Position
0
(a)
Theta
0.4
0.2
0.0
-0.2
448
Time
896
302
Position
0
(b)

FIG. 3.

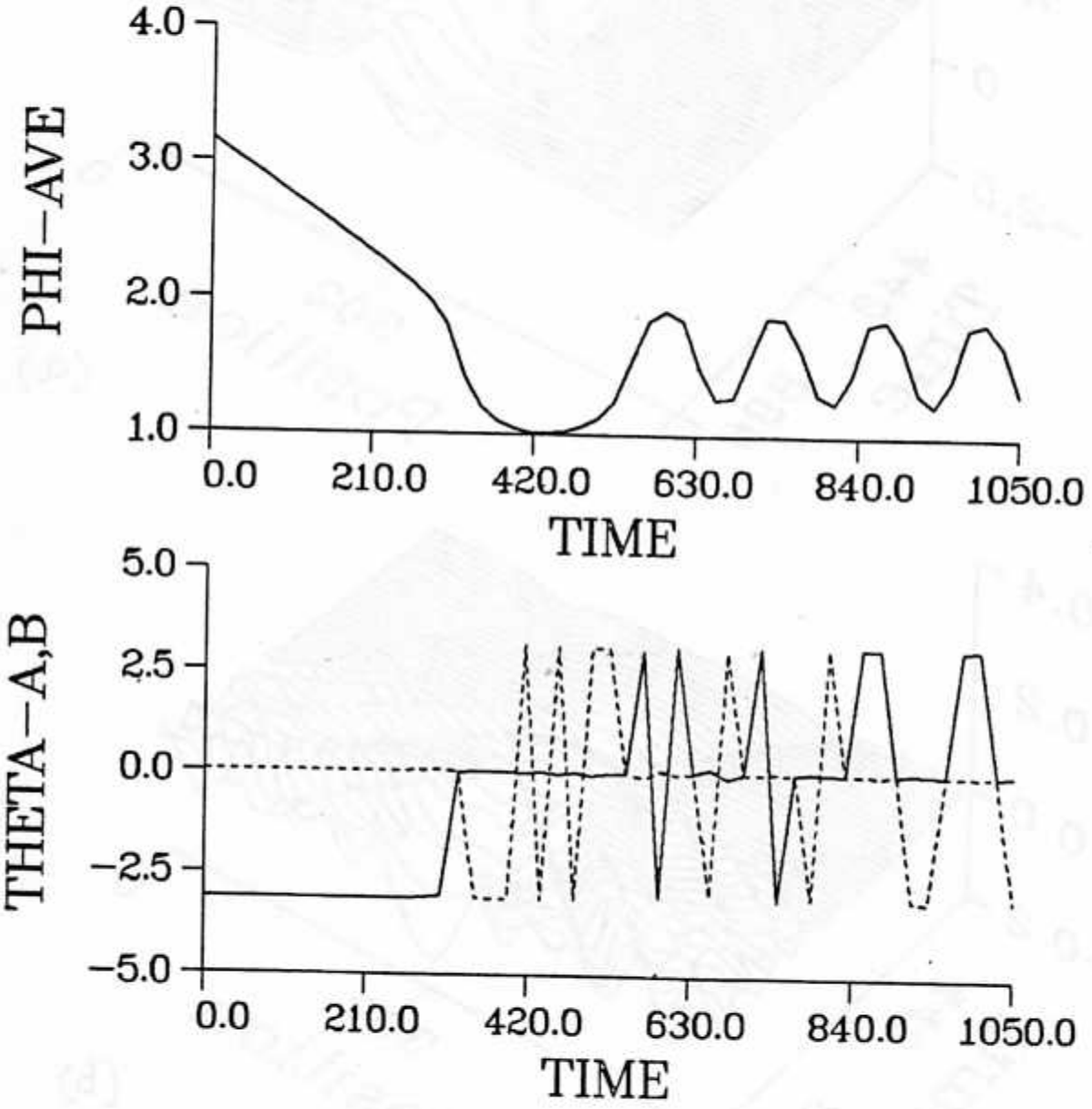
PHI–AVE
4.0
3.0
2.0
1.0
0.0
210.0
420.0
630.0
840.0
1050.0
TIME
(c)
THETA–A,B
5.0
2.5
0.0
–2.5
–5.0
0.0
210.0
420.0
630.0
840.0
1050.0
TIME
(d)

FIG. 3.

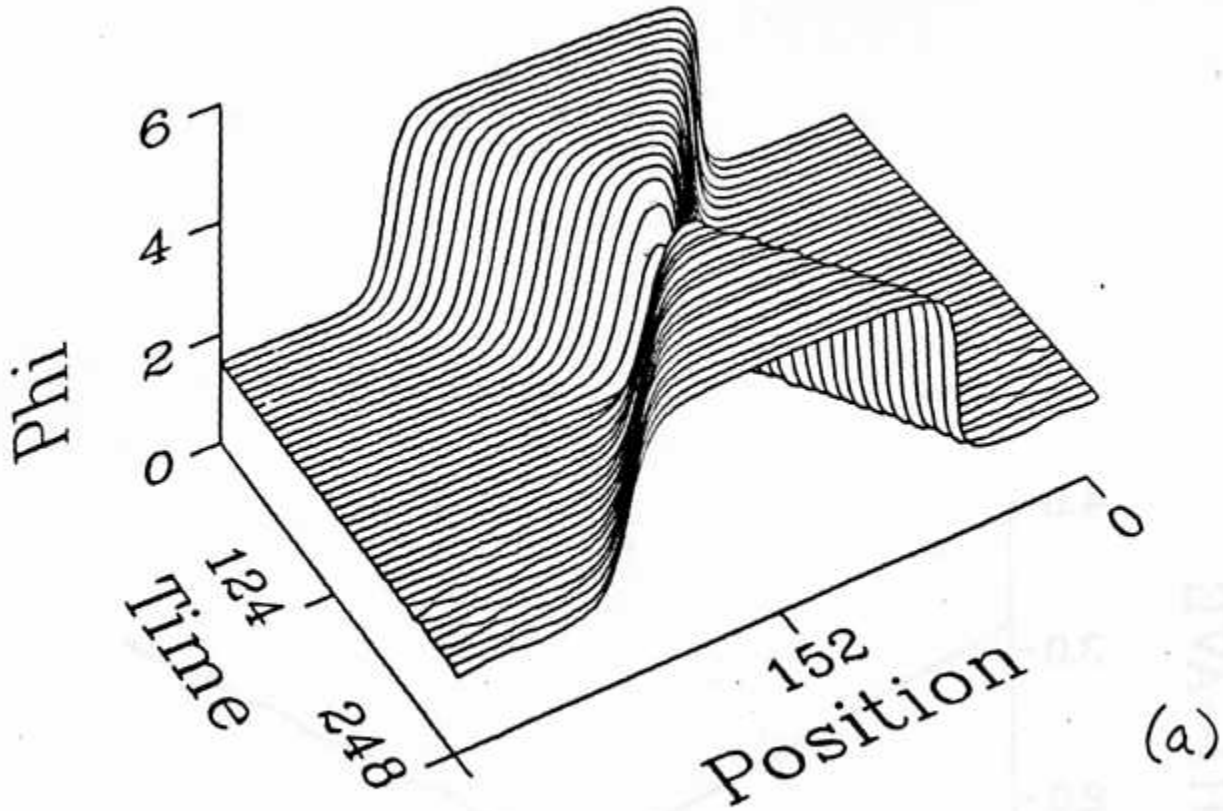
Phi
6
4
2
0
Time
124
248
152
Position
0
(a)

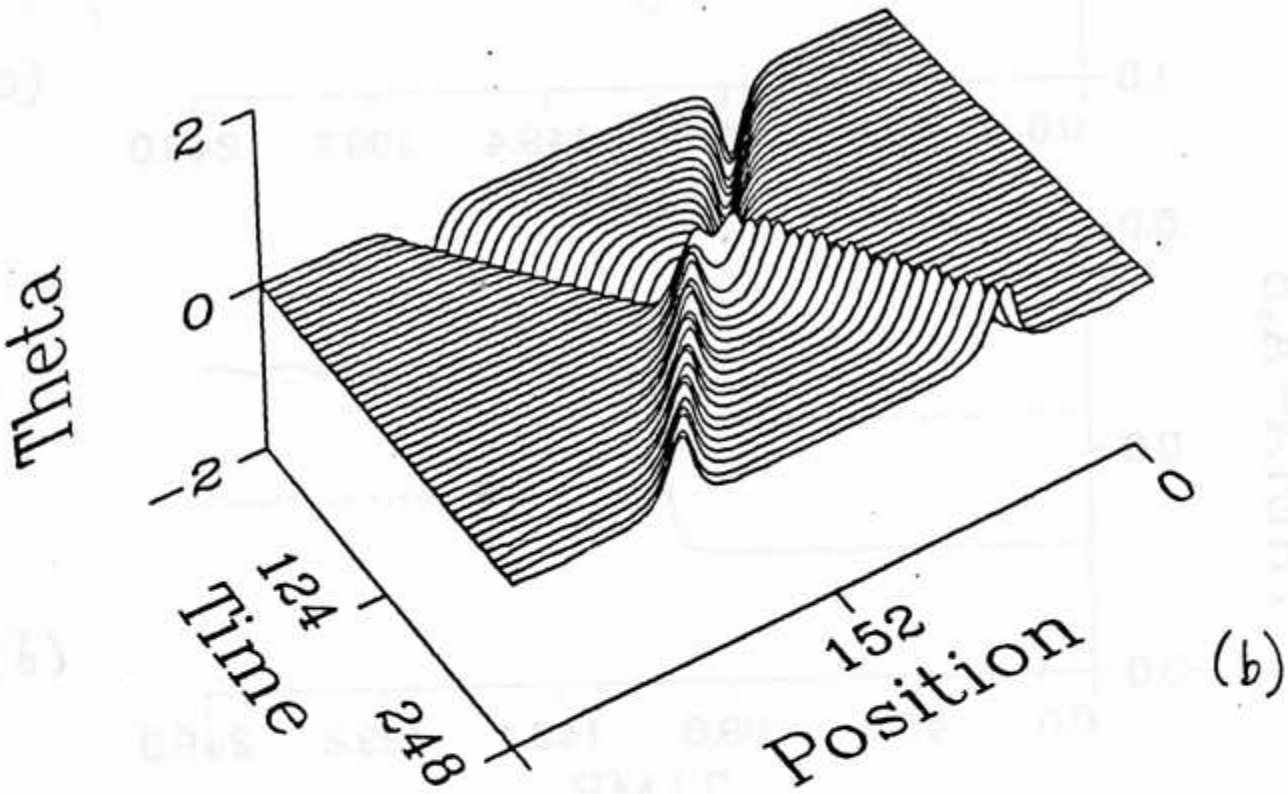
Theta
2
0
-2
Time
124
248
152
Position
0
(b)

FIG. 4.

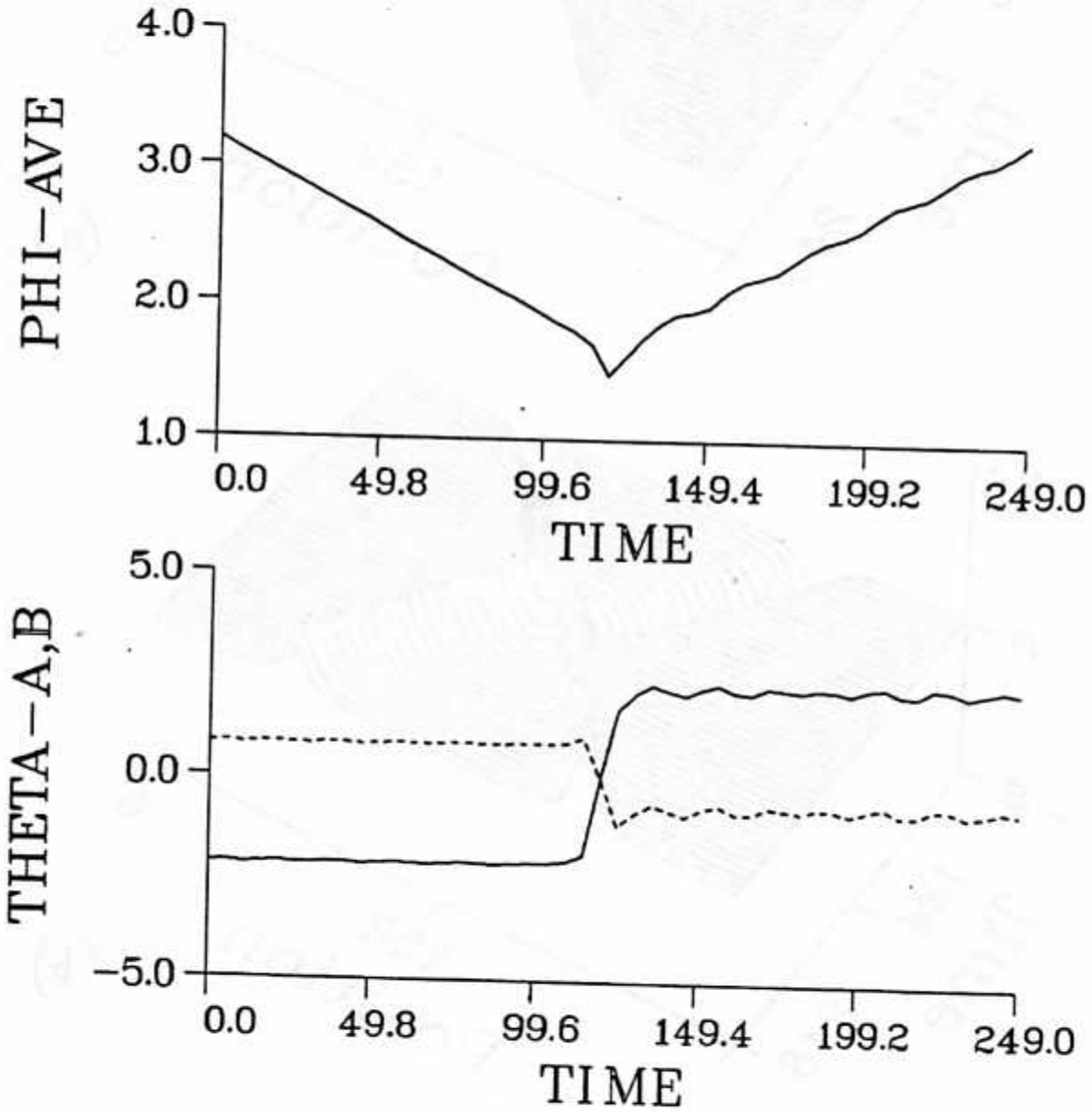
4.0
3.0
2.0
1.0
PHI-AVE
0.0
49.8
99.6
149.4
199.2
249.0
TIME
(c)
5.0
0.0
-5.0
THETA-A,B
0.0
49.8
99.6
149.4
199.2
249.0
TIME
(d)

FIG. 4.

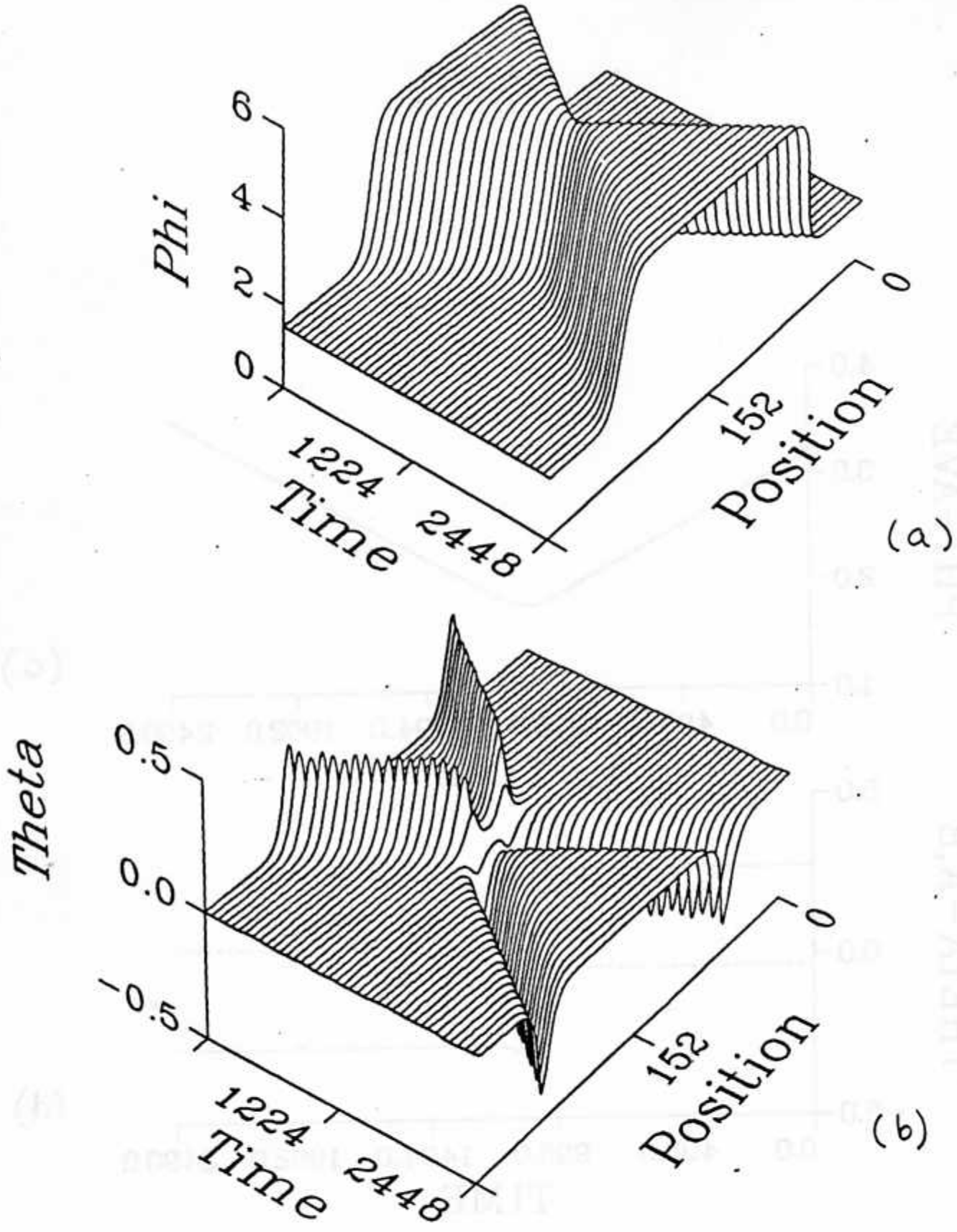
Phi
6
4
2
0
1224
2448
Time
152
Position
0
(a)
Theta
0.5
0.0
-0.5
1224
2448
Time
152
Position
0
(b)

FIG. 5.

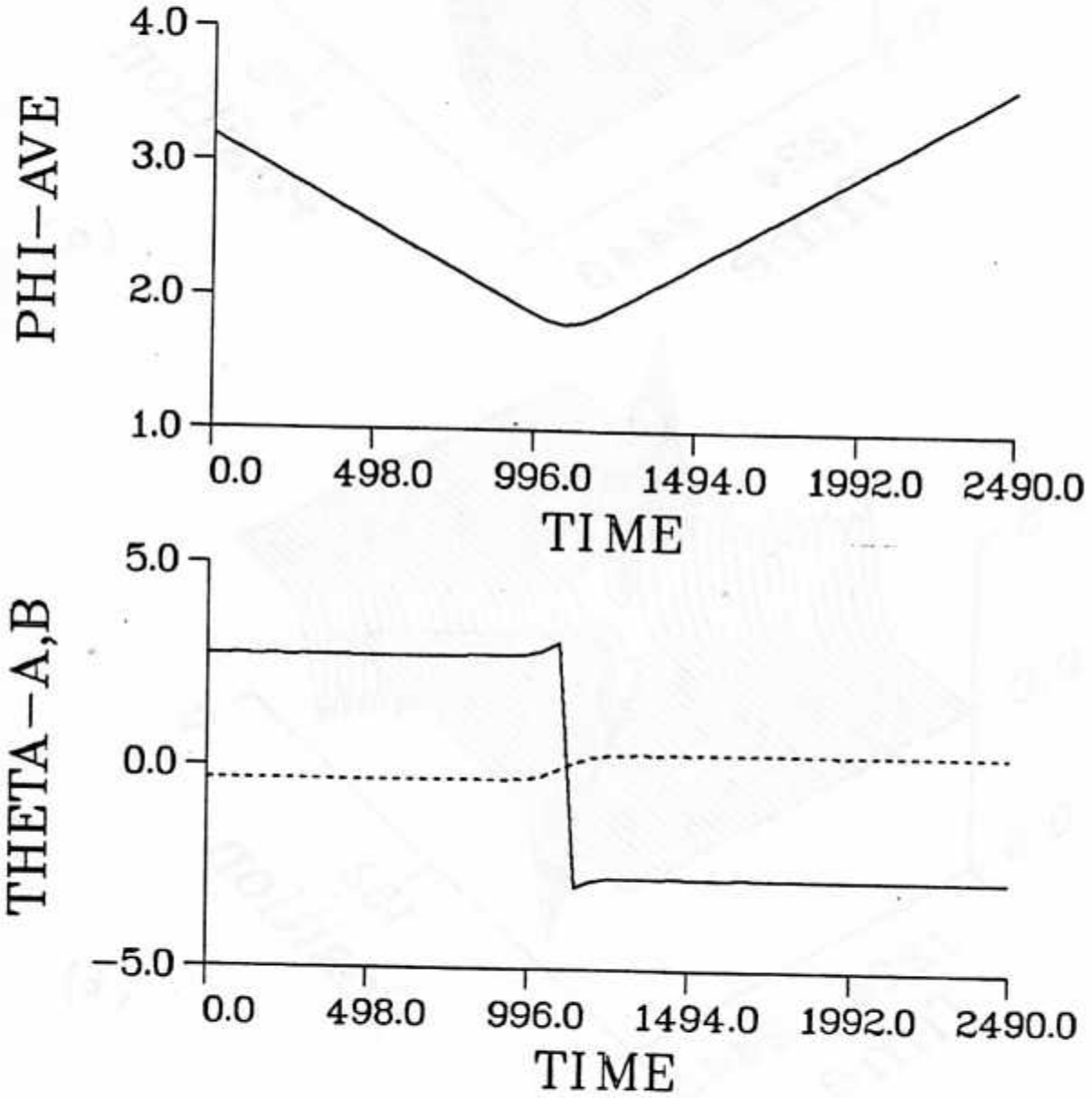
PHI-AVE
4.0
3.0
2.0
1.0
0.0
498.0
996.0
1494.0
1992.0
2490.0
TIME
(c)
THETA-A,B
5.0
0.0
-5.0
0.0
498.0
996.0
1494.0
1992.0
2490.0
TIME
(d)

FIG. 5.

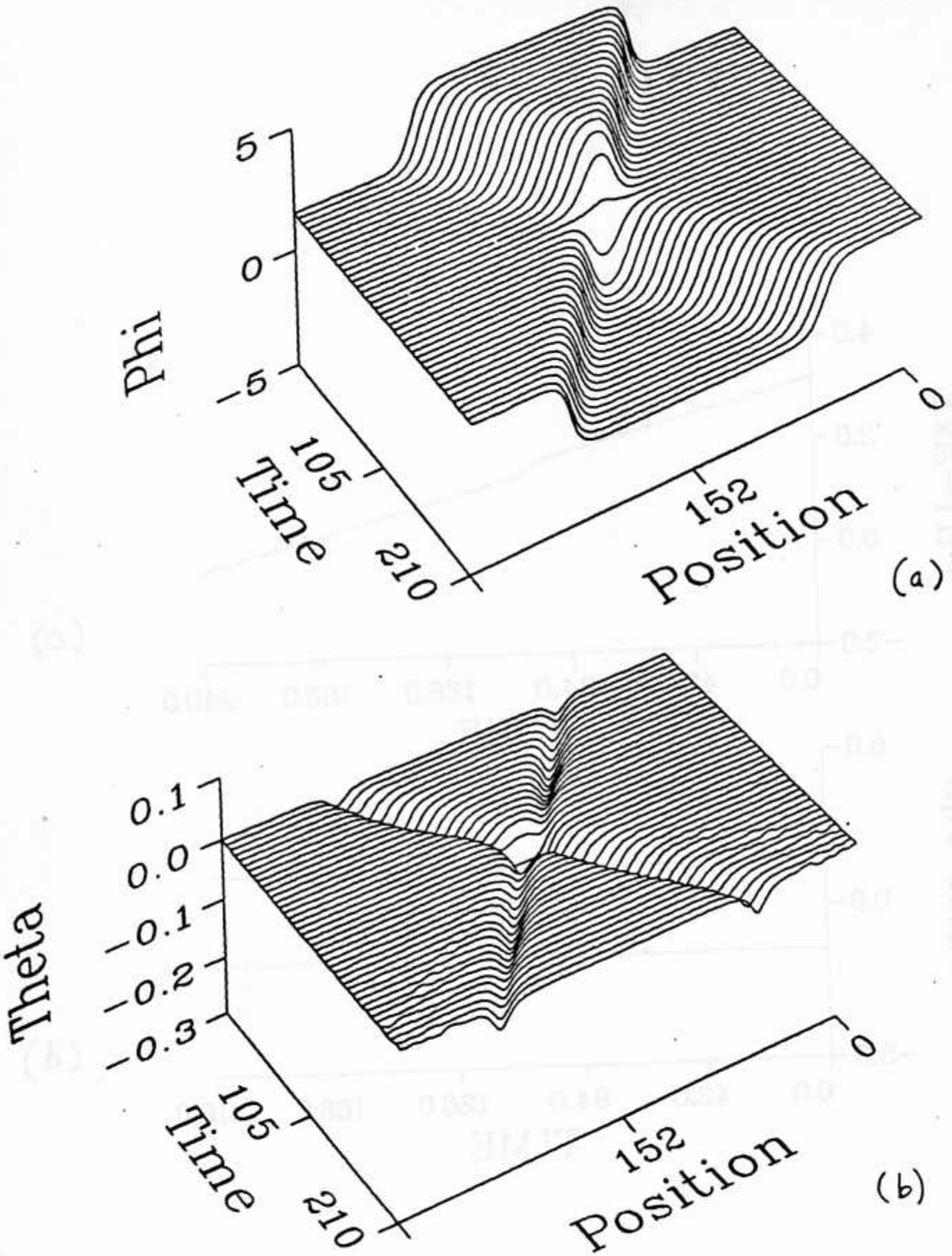
Phi
5
0
-5
Time
105
210
152
Position
0
(a)
Theta
0.1
0.0
-0.1
-0.2
-0.3
Time
105
210
152
Position
0
(b)

FIG. 6.

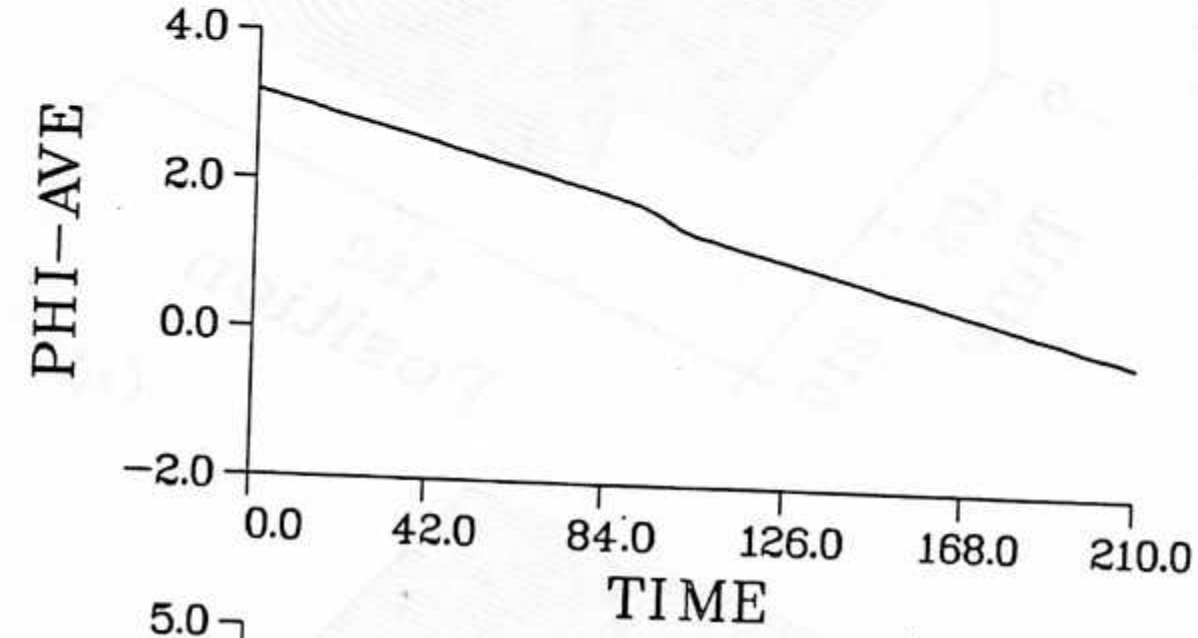
PHI-AVE
4.0
2.0
0.0
-2.0
0.0
42.0
84.0
126.0
168.0
210.0
TIME

(c)

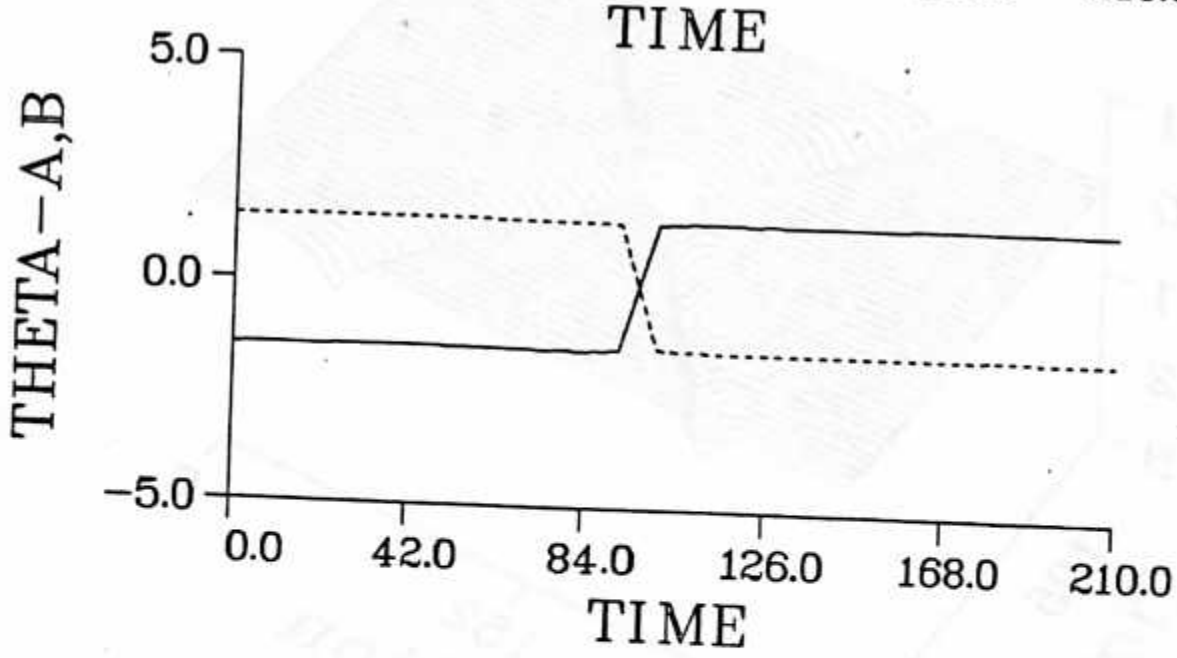
THETA-A,B
5.0
0.0
-5.0
0.0
42.0
84.0
126.0
168.0
210.0
TIME

(d)

FIG. 6.

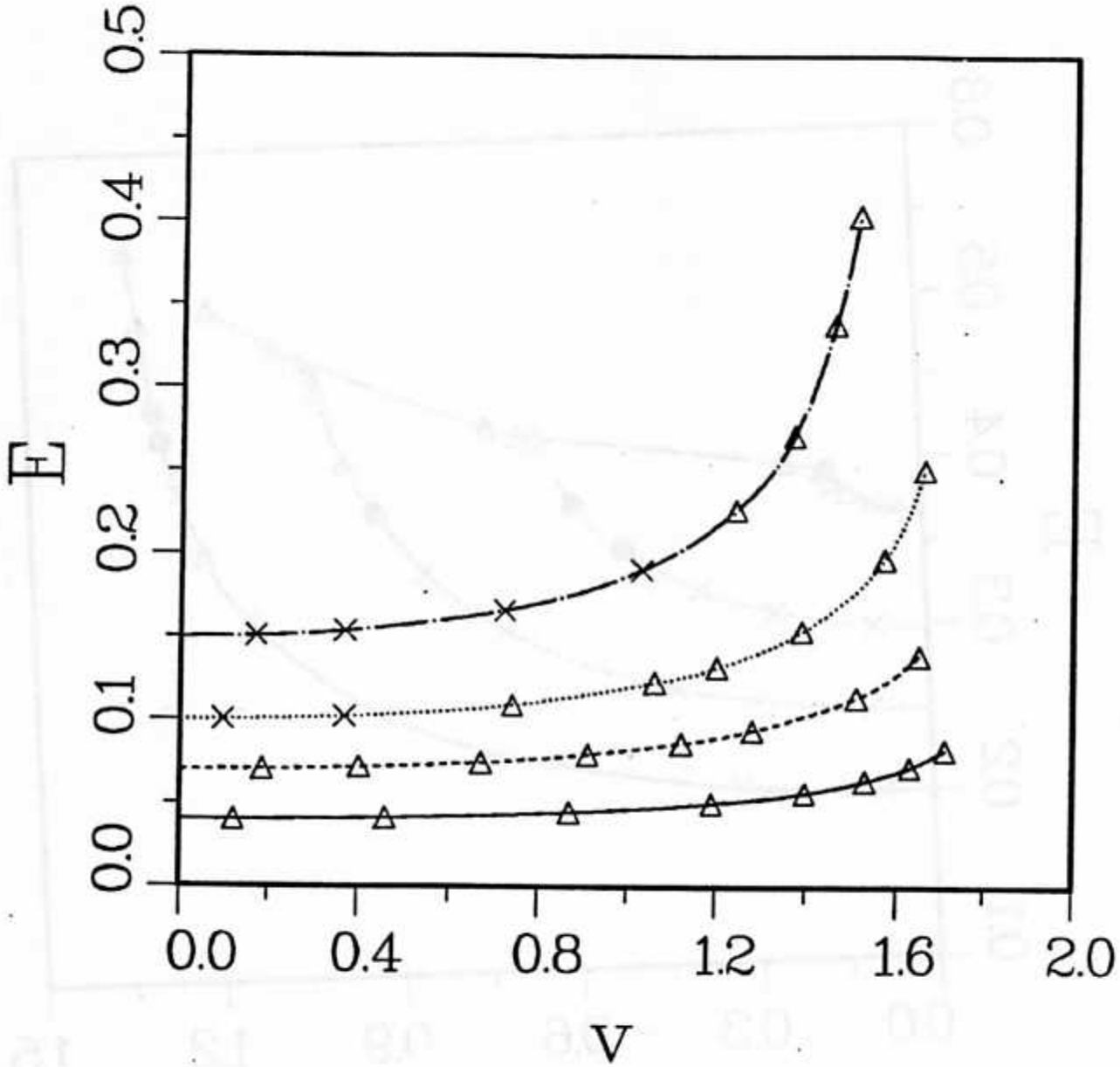

FIG. 7.

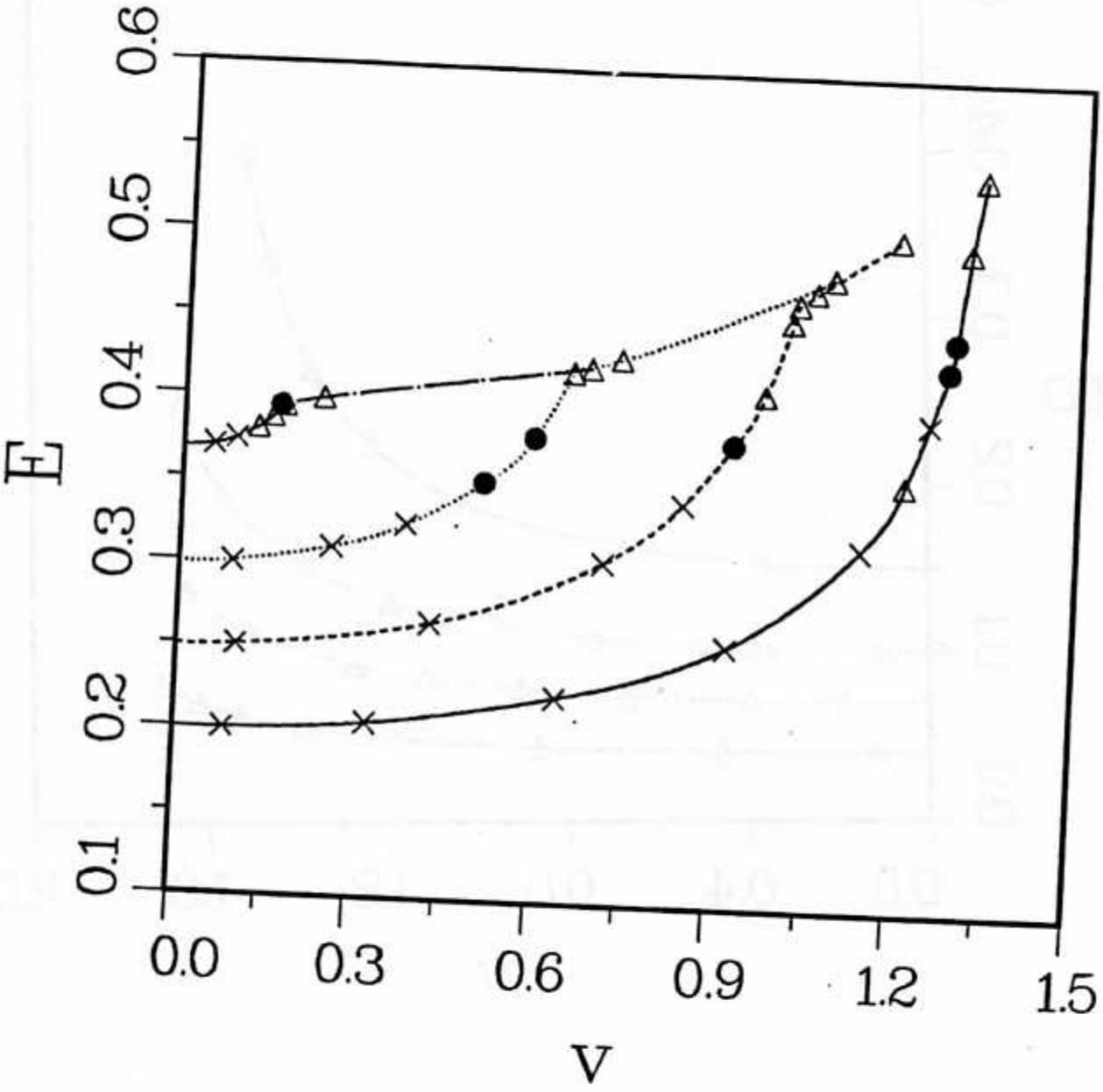

FIG. 8.

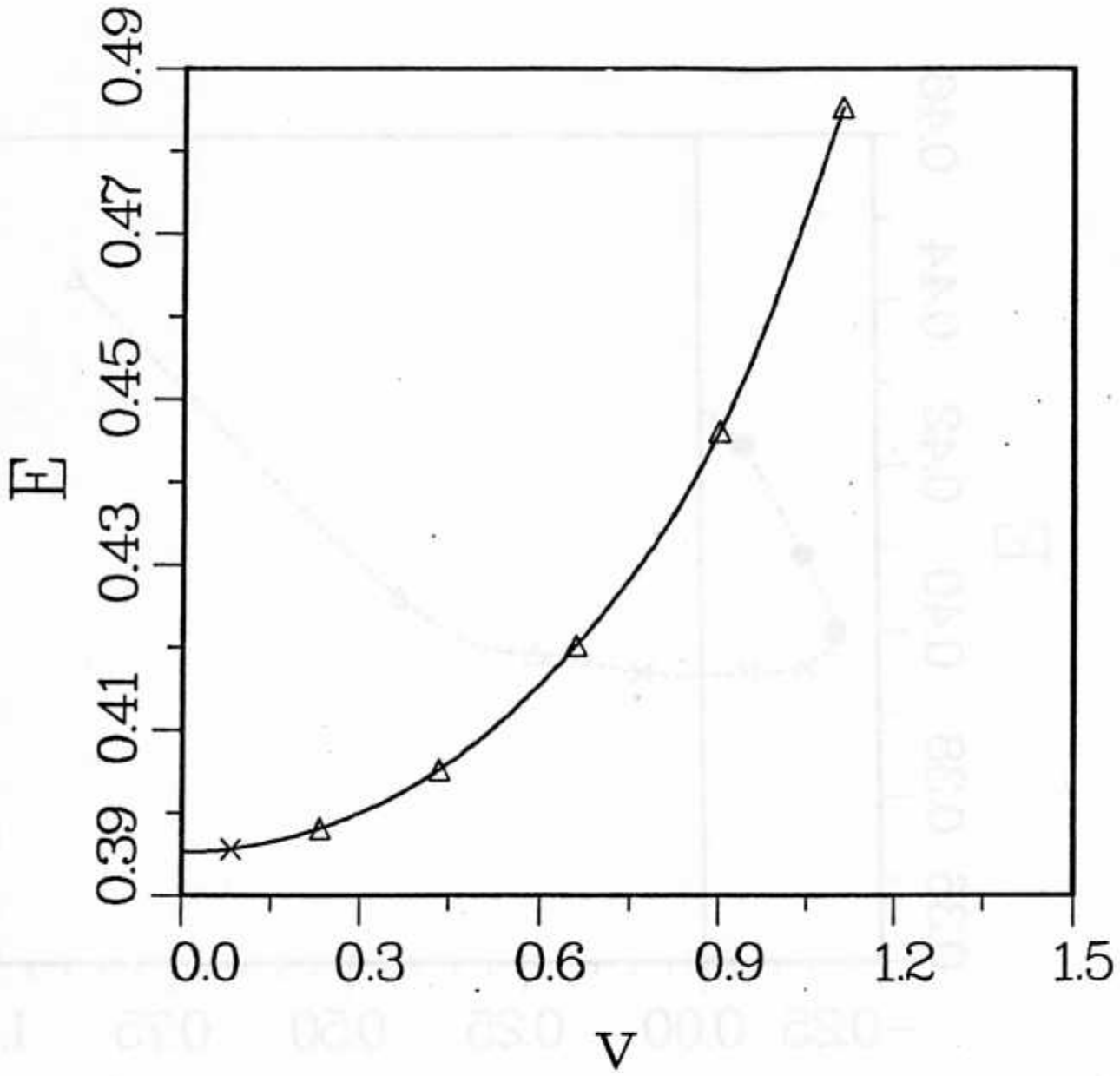

FIG. 9a.

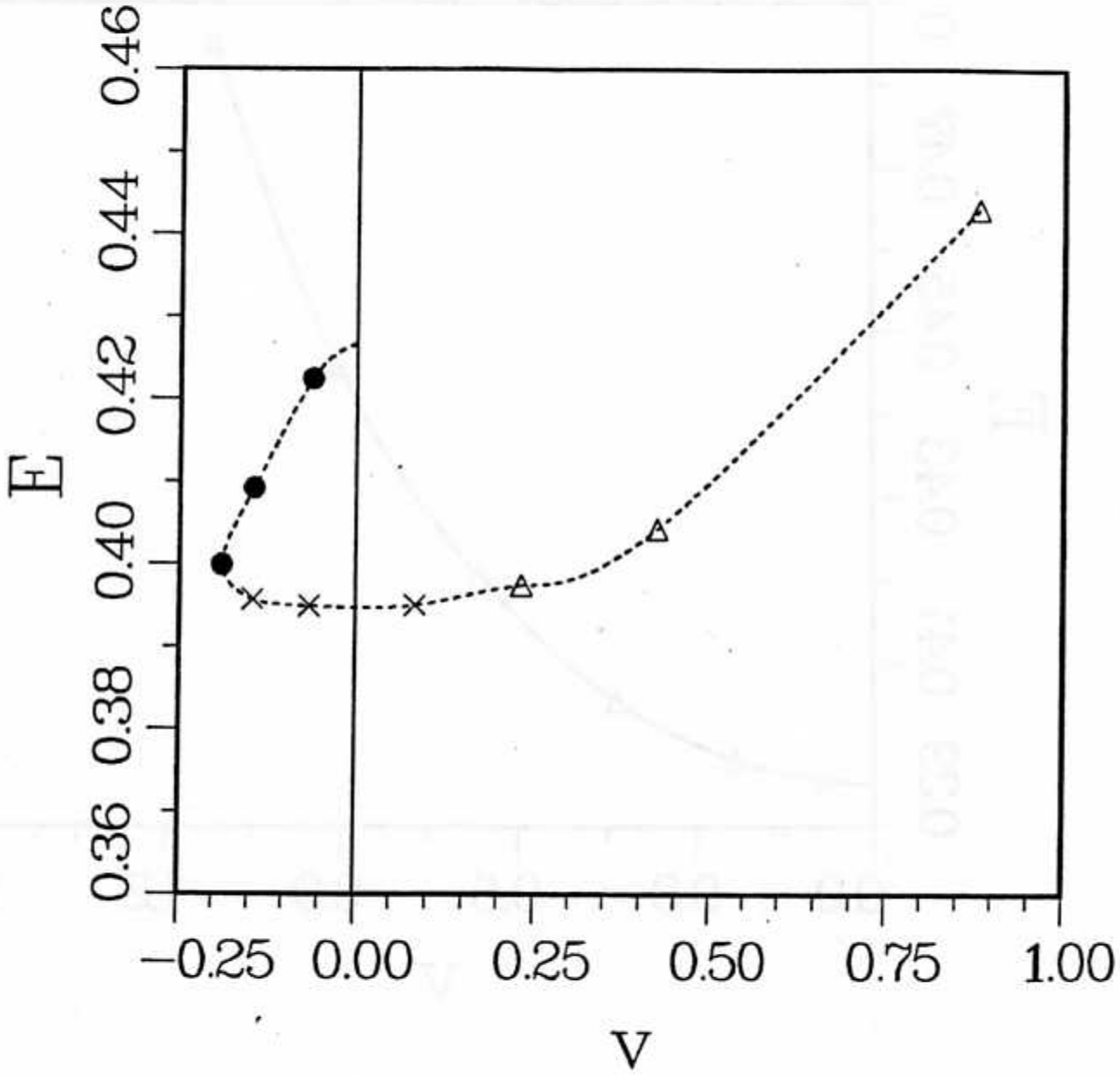

FIG. 9b.

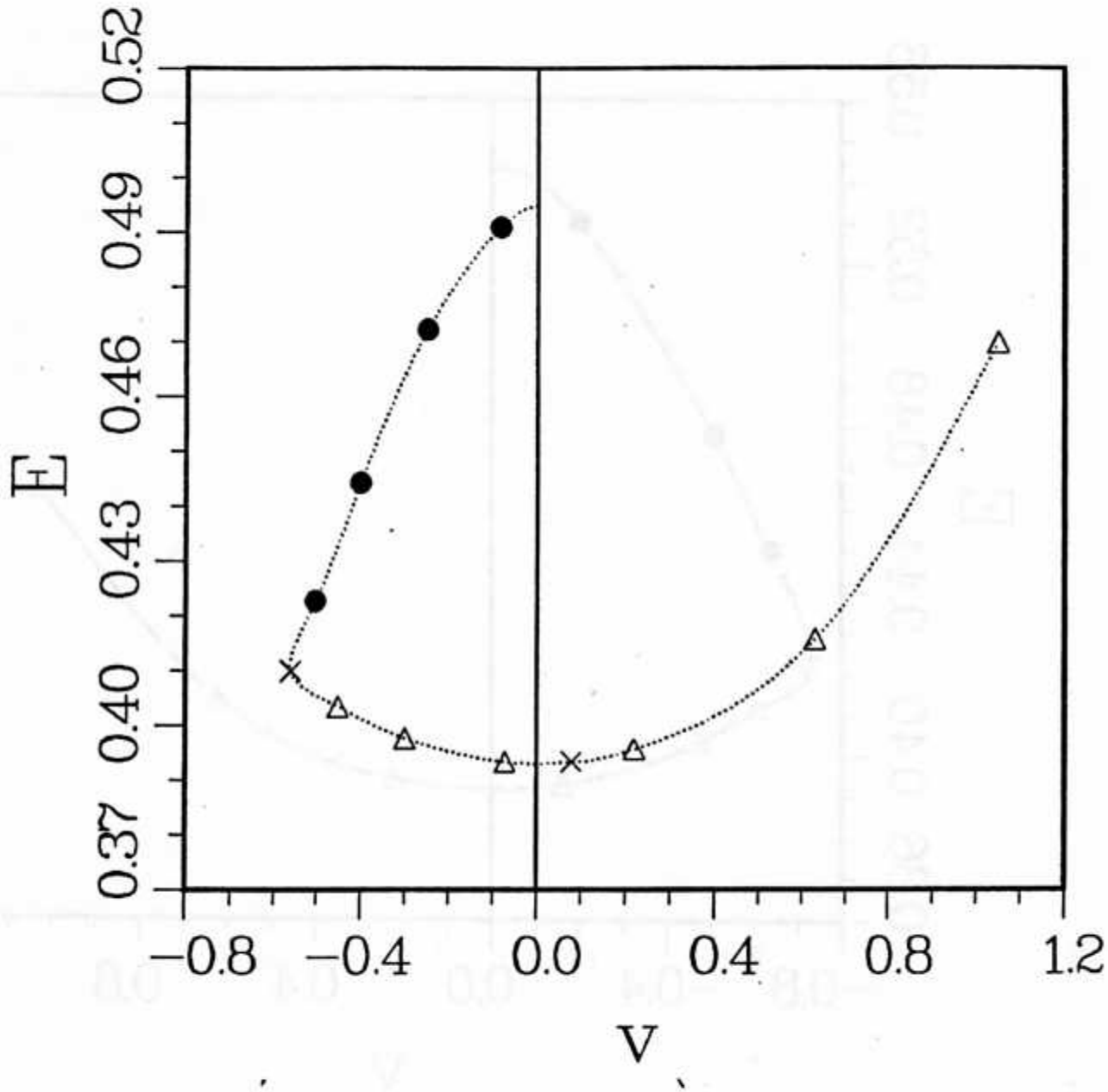

FIG. 9c.

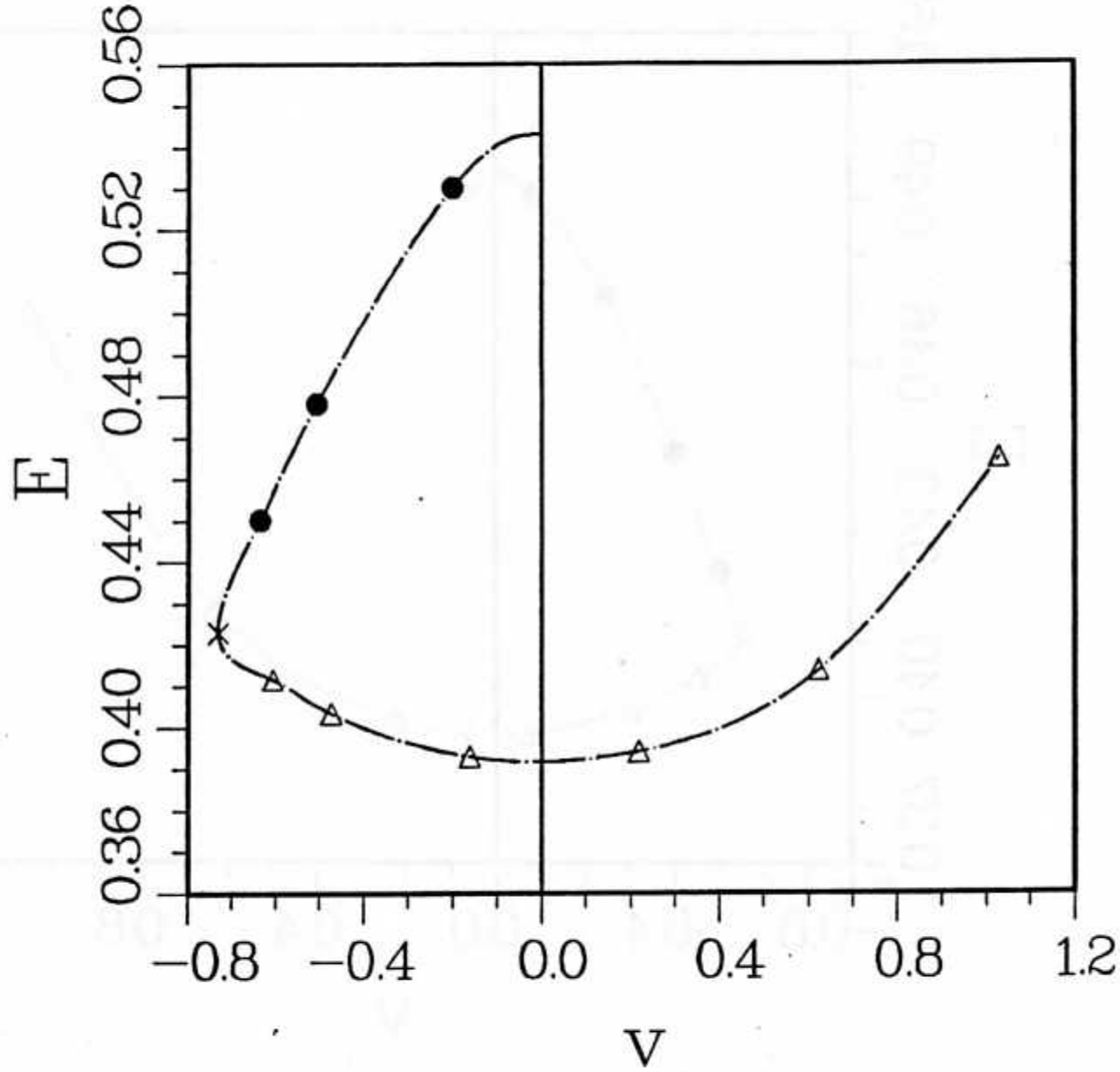

FIG. 9d.

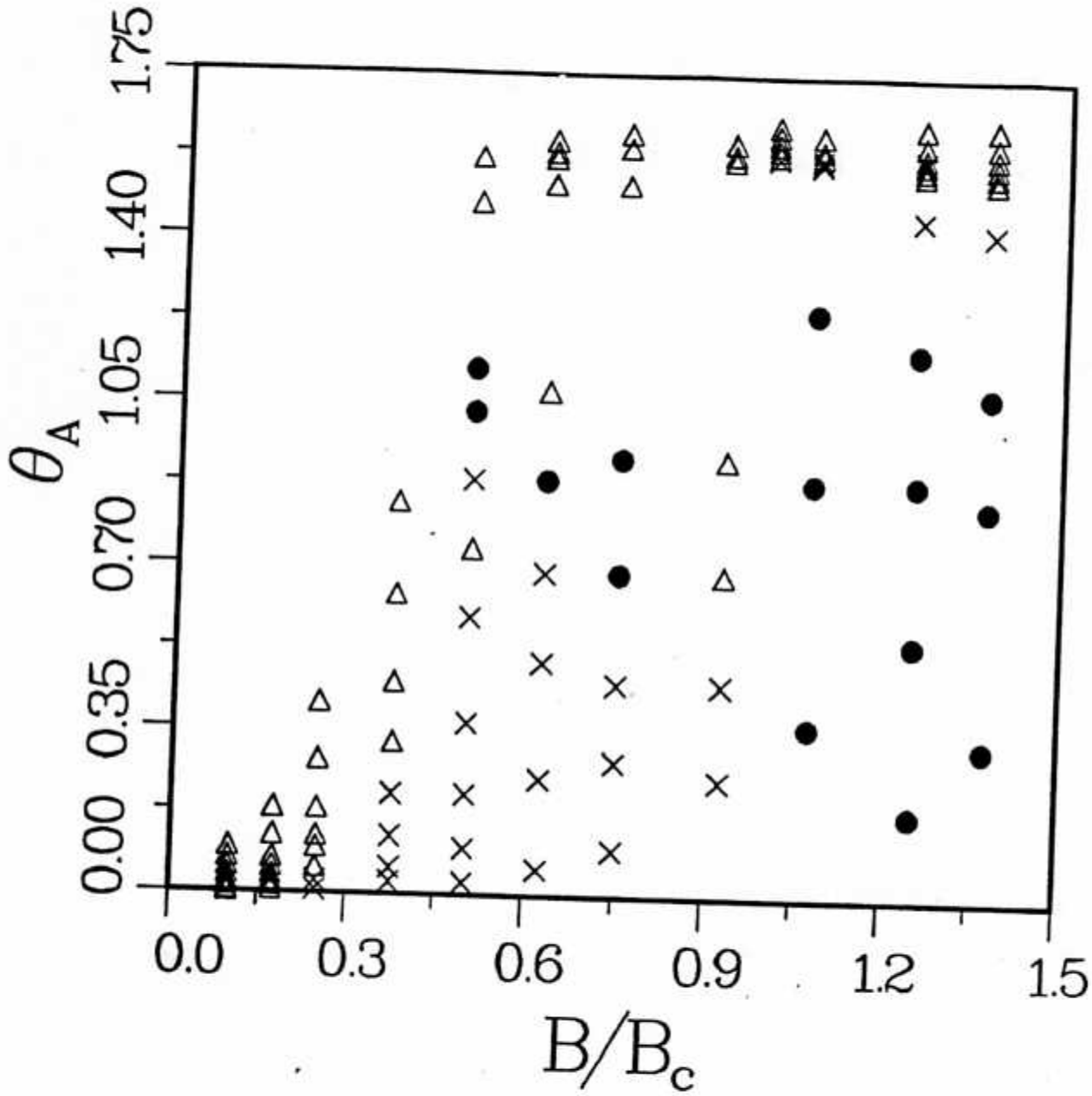

FIG. 10.